

Effects of impurity states on exchange coupling in Fe/Fe₃O₄ junctions

J. Inoue,¹ S. Honda,² H. Itoh,³ K. Mibu,⁴ H. Yanagihara,² and E. Kita²

¹*Department of Applied Physics, Nagoya University, Nagoya 464-8603, Japan*

²*Faculty of Pure and Applied Science, University of Tsukuba, Tsukuba 305-8573, Japan*

³*Pure and Applied Physics, Kansai University, Suita 564-8680, Japan*

⁴*Graduate School of Engineering, Nagoya Institute of Technology, Nagoya 466-8555, Japan*

(Received 27 March 2012; published 29 May 2012)

Exchange coupling (EC) in Fe/Fe₃O₄ junctions containing magnetic impurities and in-gap states at the interface is calculated using a formula obtained by a cleaved layer method. The model for EC is constructed by performing first-principles calculations of the electronic and magnetic states of Co, Mn, and Cr impurities on the Fe surface and those of in-gap states in a bulk γ -Fe₂O₃, which has the same lattice structure as Fe₃O₄ but contains Fe defects. We show that the effect of Co impurities on EC is opposite to that of Cr and Mn impurities and that in-gap states tend to cause parallel magnetization alignment of two ferromagnets. These results are attributed to the change in electronic states caused by the presence of impurities. Further, we compare calculated results with experimental ones obtained in Fe/Fe₃O₄ junctions and suggest that doping magnetic impurities at the interface could be a useful way to control the magnitude and sign of the EC.

DOI: [10.1103/PhysRevB.85.184431](https://doi.org/10.1103/PhysRevB.85.184431)

PACS number(s): 75.70.Cn, 71.55.-i, 73.20.-r

I. INTRODUCTION

One of the most important topics in the field of spintronics is magnetic interaction at the junction of two different ferromagnetic layers; the interlayer exchange coupling (EC) between two in magnetic multilayers^{1,2} and the exchange bias (EB) at a contact of a ferromagnet and an antiferromagnet.^{3,4} The interlayer EC between two ferromagnets (FMs) separated by a thin nonmagnetic metal layer has been interpreted to be an intrinsic phenomenon in magnetic multilayers.⁵⁻⁷ The understanding of EB, on the other hand, is rather controversial, and many mechanisms have been proposed. Although the plausible mechanisms for EC and EB could be different, it may be interesting to note that the magnitude of both EC and EB is typically ~ 1 erg/cm². It has been recently observed that α -Fe/Fe₃O₄ (magnetite) and α -Fe/ γ -Fe₂O₃ (maghemite) junctions show antiparallel (AP) and parallel (P) EC between two FMs, respectively.⁸⁻¹⁰ Furthermore, EC in nanocomposite magnets attracts considerable interest for the fabrication of stronger permanent magnets than rare-earth-based permanent magnets.^{11,12}

As the interlayer EC in magnetic multilayers plays an important role in technological applications, control of the EC between two ferromagnets may lead to new applications of hard and soft magnets. For example, since the magnitude of EC in the Fe/Fe₃O₄ junction is about 1 erg/cm² comparable to that in Co/Ru/Co trilayers,¹³ Fe/Fe₃O₄ junctions may be used as synthetic antiferromagnets when the magnetizations of the Fe and Fe₃O₄ layers have been designed to be compensated by each other. Control the EC in Fe/Fe₃O₄ junctions by doping magnetic impurities such as Co and Mn at the interface of the junction has been previously attempted, and it showed that the EC depends on the type and concentration of the impurity.¹⁴ Despite these efforts to control the EC, the mechanism of the AP and P coupling in Fe/Fe₃O₄ and Fe/ γ -Fe₂O₃ and the origin of the variation in EC as a result of doping with magnetic impurities at the interface have not yet been clarified.

The first-principles method can be useful for studying the EC of two FMs by comparing the total energy of P and AP

magnetization alignments of the FMs. Several studies have reported the EC calculated by the first principles method for Fe/Fe₃O₄,¹⁵ Fe/Nd₂Fe₁₄B,¹⁶ and magnetic semiconductor junctions.¹⁷ However, the calculated EC is one or two orders of magnitude larger than the observed values.^{8-10,18} The calculated values may correspond to the intrinsic interaction between two magnetic moments at an ideal junction and may be weakened by extrinsic causes. Simulation of the magnetization in nanocrystalline magnets also requires smaller EC than the magnetic interaction in bulk magnets in order to explain the observed magnetization process.^{19,20} Such discrepancy between the EC calculated using the first-principles method and the observed value has been reported for magnetic trilayers as well, in which a nonmagnetic spacer exists between two FMs.^{21,22} Both the intrinsic and extrinsic origins of the EC have been reported for Fe/MgO/Fe tunnel junctions.²³⁻²⁵

In directly coupled ferromagnetic junctions without a nonmagnetic spacer, distinguishing between the extrinsic and intrinsic mechanisms may be difficult. To understand the intrinsic mechanism of EC, it is necessary to perform calculations considering how the EC is related to the electronic state of the junction. In the present work, we focus on the role of magnetic impurities at the interface on the EC in Fe/Fe₃O₄ and Fe/ γ -Fe₂O₃ junctions. Examining the dependence of EC on the impurity concentrations may facilitate identification of the intrinsic EC from the extrinsic one. However, possible structural disorder existing extrinsically at oxides interface may hinder us from constructing realistic models for the EC. To visualize the role of the electronic states of magnetic impurities on the EC, we adopt simple models for the junction and impurities. As for magnetic impurities, we examine the effect of Co, Mn, and Cr impurities introduced at the Fe interface and in-gap states at the Fe₃O₄ interface caused by excess oxygen and/or defects of Fe ions. In addition, because Fe₃O₄ is believed to be half-metallic (HM),^{26,27} and γ -Fe₂O₃ an insulating oxide,²⁸ we study the effects of the electronic states of oxides (half-metallic or insulating) on the EC. Thus we perform first-principles calculation for the electronic and

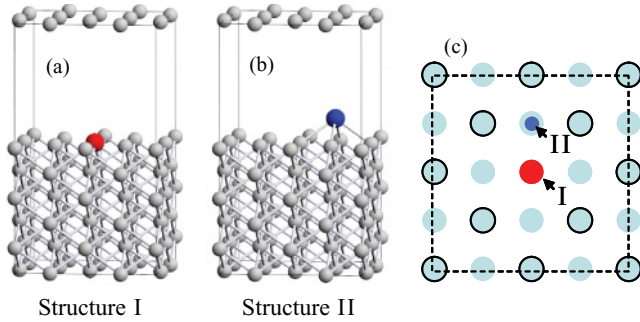


FIG. 1. (Color online) Unit cell used in the first-principles calculations, (a) side view of structure I in which an impurity is located within the surface layer, (b) side view of structure II in which an impurity is located above the surface layer, and (c) top view of the impurity's location in both site I and II.

magnetic states of Co, Mn, and Cr impurities on the Fe surface and the in-gap states of γ -Fe₂O₃. Based on the results, we construct a simple model for junctions of two FMs with magnetic impurities and in-gap states. The EC is calculated by adopting a formula obtained in the cleaved layer method; it is identical to that obtained using the force theorem.^{29–33}

The paper is organized as follows. In the next section, we show results obtained in the first principles calculations for electronic and magnetic states of Co, Mn, and Cr impurities on the Fe surface and for electronic states of γ -Fe₂O₃. In Sec. III, a simple model for the EC in junctions with magnetic impurities or in-gap states at the interface is presented. Calculated results of the EC are presented in Sec. IV, which is followed by a section containing comparison of the results with experimental results and related discussions. Conclusions are presented in the final section.

II. FIRST-PRINCIPLES STUDY

We first present results of the first-principles study on the density of states (DOS) and magnetic moments of impurities on the Fe surface, and the DOS of maghemite (γ -Fe₂O₃) with excess Fe or O ions. The calculation is performed using the Vienna *ab initio* simulation package (VASP)³⁴ in which the PAW (projected augmented wave) pseudopotential and a spin-polarized GGA (generalized gradient approximation)-PW (Perdew-Wang) method, including a correction of the Coulomb interaction U , are adopted. The cutoff value of the plane waves is 400 eV. U is assumed to be zero for transition metals and 4.5 eV for the Fe ions in maghemite. Although the value of U cannot be determined unambiguously for transition metal oxides, we adopt the value of U used previously for Fe₃O₄.¹⁵ The k -point sampling is $(9 \times 9 \times 3)$ in Monkhorst-Pack mesh for maghemite and $(9 \times 9 \times 5)$ for calculation of the impurity state on the Fe surface.

A. TM impurity on Fe surface

Figures 1(a) and 1(b) show unit cells used in the calculation for an impurity atom within the surface layer of Fe and above the surface layer, respectively. Hereafter, we refer to the former (latter) unit cell as structure I (structure II). The lattice constants of structures I and II are taken to be 8.0327,

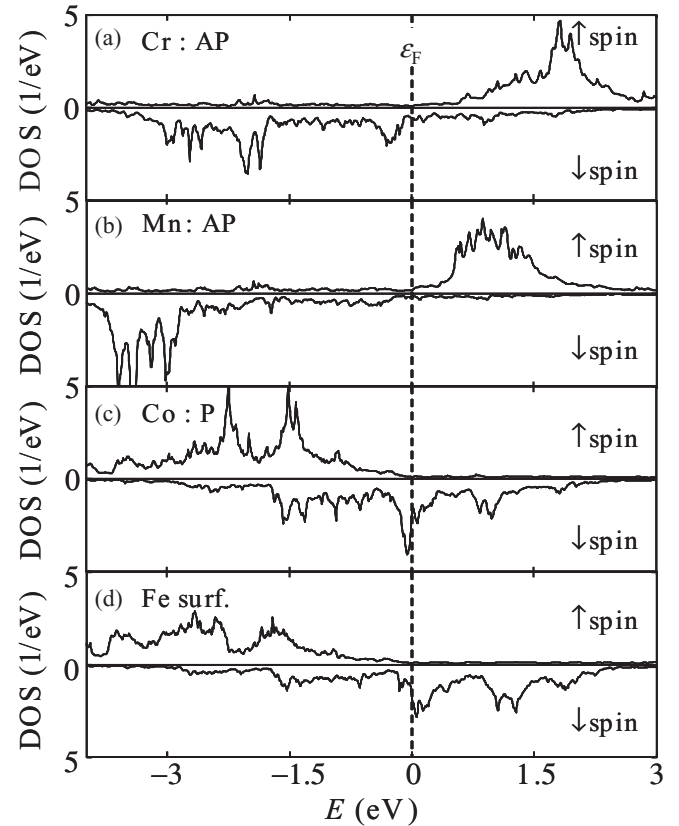


FIG. 2. Calculated results of local density of states (DOS) of impurity (a) Cr, (b) Mn, (c) Co in structure I, and (d) local DOS of Fe in the surface layer. Cr and Mn impurities have magnetic moments antiparallel (AP) to Fe moment, while Co impurity has parallel (P) moment. Fermi energy is located at $E = 0$.

8.0327, and 14.2000 Å, including a vacuum layer. Figure 1(c) shows a cross section of the unit cell. The unit cell contains six atomic layers of Fe and a vacuum layer, and therefore has 48 atomic sites. We also performed calculations for structure II with a half-size unit cell.

Calculated results for the local density of states (DOSs) of Co, Cr, and Mn impurities for structure I are shown in Fig. 2. For both structures I and II, Co impurity has positive magnetic moment (parallel to Fe moment), while Cr and Mn impurities have negative magnetic moments (antiparallel to Fe moment), as shown in Table I. Therefore, exchange splitting of the local DOSs of Cr and Mn impurities is opposite to that of the DOS of Fe. Because the magnetic moments of Cr and Mn are large, they show localized-moment character, and their local DOSs have effectively a narrower bandwidth than that of

TABLE I. Impurity moments in units of μ_B per atom calculated by the first-principles method. Results of structure II with smaller unit cell (u.c.) are also presented. Here, + (–) indicates moments parallel (antiparallel) to that of the Fe atom.

impurity	structure I	structure II	small u.c.
Co	+1.86	+1.92	+1.9(–1.6)
Mn	–3.73(+0.44)	–3.80(+3.65)	–3.7(+3.5)
Cr	–3.35(+0.82)	–3.53	–3.3(+2.5)

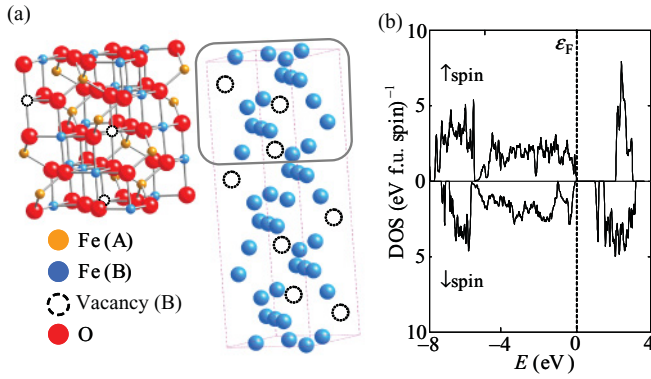


FIG. 3. (Color online) (a) Unit cell of bulk maghemite $\gamma\text{-Fe}_2\text{O}_3$. The figure on the left shows one third of the unit cell as enclosed by a solid curve in the right figure. (b) Calculated results of DOS of maghemite.

Fe atoms. Magnetic moment of Co impurity is positive and the local DOS hybridized strongly with Fe bands. The tendency is stronger for structure I than for structure II, because of a small coordination number around the impurity in structure II.

Calculated results of the magnetic moments of impurities are shown in Table I. Values in parentheses are those in unstable states. Magnitude of the magnetic moments in the stable states is almost independent of the structure. We find that Cr and Mn impurities have large negative moments, similar to impurity moments in transition-metal alloys.^{35–39}

B. Maghemite

To study the effects of excess or deficient oxygen in the magnetite layer on EC, it is important to know the preferential sites in which the excess or deficient oxygen resides. Because such structural information is lacking at present and random selection of defect sites of oxygen or iron may yield unreliable results due to the complex lattice structure of magnetite, we perform the first-principles calculation for $\gamma\text{-Fe}_2\text{O}_3$ (maghemite). The detailed structure of maghemite has recently been reported.²⁸ Stability of vacancy ordering has also been confirmed by first-principles study.⁴⁰

Maghemite, which is a ferrimagnet used in magnetic recording media, has $D_4^8\text{-}P4_32_12$ symmetry with lattice constants $a = 8.394$ and $c = 25.182$ Å. Ionic arrangement of maghemite is expressed as $\text{Fe}^{3+}[\text{Fe}_{5/3}^{3+}\square_{1/3}]\text{O}_4^{-2} = \text{Fe}_{8/3}\text{O}_4 = \text{Fe}_2\text{O}_3$, where \square indicates a vacancy site. The unit cell contains 64 Fe and 96 O ions and is shown in Fig. 3(a).

Figure 3(b) shows the calculated result of maghemite DOS. The Fermi energy is located within the energy band gap. Because the width of the energy gap is spin dependent, maghemite is a ferrimagnetic insulator. The DOS of maghemite consists of three regions: above the Fermi energy are mainly exchange-split Fe ions, the middle part is composed of mainly oxygen p orbitals, and the lowest part is again composed of the exchange-split Fe ions. The most important aspect is that a split-off state exists in the down spin state just below the conduction band. The split-off state may have originated from ion defects or vacancy sites in the lattice, as confirmed by further calculations for excess O_2 and excess Fe_2 atoms in maghemite.

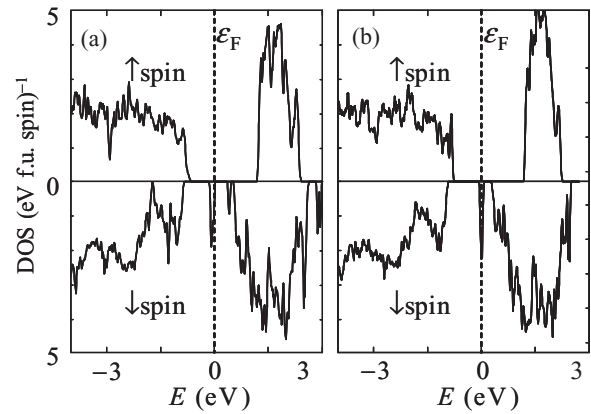


FIG. 4. Calculated results of DOS for (a) maghemite with two excess Fe atoms and (b) maghemite with two excess oxygen atoms. Fermi energy is located at $E = 0$.

Figures 4(a) and 4(b) show the results of $\text{Fe}_{66}\text{O}_{96}$ (excess Fe) and $\text{Fe}_{64}\text{O}_{98}$ (excess O), respectively. We observe that a sharp peak exists at the Fermi energy in the down spin bands. These peaks are identified to be indicative of the in-gap states caused by excess ions. Thus, we expect such split-off states or in-gap states to exist at the interface of Fe/ Fe_3O_4 because the junctions are usually fabricated under an excess oxygen environment.

Quite recently, *ab initio* study on the electronic states of oxygen defect Fe_3O_4 has been reported.⁴¹ The results show that in-gap states appear in the local DOS of the minority spin state of both A- and B-site Fe. It has been reported that the magnetic moments of A- and B-site Fe are reduced by 0.2 and $0.41 \mu_B/\text{Fe}$, respectively, due to the in-gap states.

III. MODEL FOR EXCHANGE COUPLING

A. Junction model

We construct a model adopting two basic assumptions; a flat interface at the junction and a weak overlap of wave functions of two FMs. The latter assumption is justified when we note that the interface of Fe/ Fe_3O_4 is highly resistive.⁴⁶ The junctions are formed between two FMs having half-infinite simple cubic lattices with a (100) plane at the interface, as shown schematically in Fig. 5(a). The left (L) and right (R) FMs correspond to Fe and Fe_3O_4 , respectively. The electronic state is modeled as follows. Our previous first-principles study on the electronic state of Fe/ Fe_3O_4 showed that A-site Fe seems to be unrelated to the coupling energy, and Mössbauer

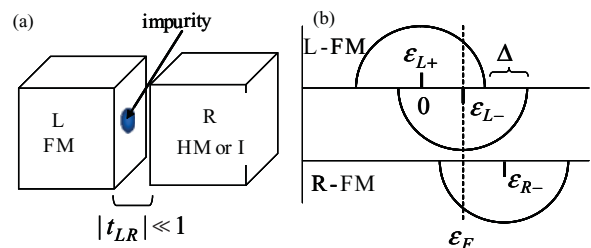


FIG. 5. (Color online) Schematic of the (a) junction model and (b) the electronic states of the junction used in the calculation.

study indicates the interface layer of Fe_3O_4 may be dominantly formed by B-site Fe.¹⁵ Therefore the electronic state of L-FM is approximated using an exchange-split single orbital tight-binding model, and that of R-FM is approximated by a half-metallic single orbital model corresponding to B-site Fe. The majority spin band of R-FM is neglected for simplicity because of a strong exchange splitting of Fe ions in Fe_3O_4 . The exchange splitting of L-FM is denoted by Δ , and a nearest neighbor hopping integral t is adopted for both L- and R-FMs. The model DOSs of the junction is presented in Fig. 5(b). The hopping integral t_{LR} between L and R layers is assumed to be sufficiently smaller than t to apply the second order perturbation for the EC with respect to t_{LR} . It should be noted that the magnetization of Fe_3O_4 is dominated by the magnetic moments on B-site Fe, and therefore the magnetization direction of L-FM in the model is the same as that in Fe_3O_4 .

Because of the perfectly flat interface of the junction, the translational invariance holds along the interface plane, and both in-plane momentum k_{\parallel} and atomic layer index ℓ are used to describe the electronic states of the junction. When there is no disorder in the junction, the energy state within a single layer is characterized by an energy-dispersion relationship, $\varepsilon(k_{\parallel}) = -2t(\cos k_x + \cos k_y)$, which is assumed to be the same for L and R layers. Hereafter, t is taken as the unit of energy.

Because the model neglects A-site Fe, the in-gap states on A-site Fe predicted for oxygen-deficient Fe_3O_4 are ignored.⁴¹ However, we expect that states in oxygen-deficient Fe_3O_4 play a less important role due to the oxygen-rich atmospheres in the sample fabrication process; we will discuss effects of such states in Sec. V.

B. Exchange coupling

The general expression of EC has been obtained by a cleaved layer method or by the force theorem^{29–33} in which the expression is formulated by considering the insertion of a cleaved layer at the interface. In the present model, the cleaved layer corresponds to the interface of the junction. When the hopping integral t_{LR} between L and R layers is treated in the second-order perturbation, the exchange coupling J is simplified to

$$J = E_{\text{P}} - E_{\text{AP}} \quad (1)$$

$$= -\frac{t_{\text{LR}}^2}{\pi} \text{Im} \sum_{k_{\parallel}} \int_{-\infty}^{\varepsilon_{\text{F}}} d\varepsilon [G_{\text{L}+}(\varepsilon, k_{\parallel}) - G_{\text{L}-}(\varepsilon, k_{\parallel})] \times [G_{\text{R}+}(\varepsilon, k_{\parallel}) - G_{\text{R}-}(\varepsilon, k_{\parallel})] \quad (2)$$

using the surface Green's function of L(R) magnet,

$$G_{\text{L(R)}\sigma}(\varepsilon, k_{\parallel}) \quad (3)$$

$$= \frac{1}{z - \varepsilon_{\text{L(R)}\sigma} - \Sigma_{\text{L(R)}\sigma}(z) - \varepsilon(k_{\parallel}) - t^2 g_{\text{L(R)}\sigma}(z, k_{\parallel})}, \quad (4)$$

with $z = \varepsilon + i0$ and spin $\sigma = +(-)$, $+$ for majority and $-$ for minority spins. $\Sigma_{\text{L(R)}\sigma}(z)$ is self-energy that includes the effects of disorder on the surface layer of L(R) magnet. The translational invariance within the surface layer may be recovered by an averaging procedure over the distribution of randomness in the layer. When $\Sigma_{\text{L(R)}\sigma}(z) = 0$, the Green's function $G_{\text{L(R)}\sigma}(\varepsilon, k_{\parallel})$ reduces to the surface Green's function

$g_{\text{L(R)}\sigma}(\varepsilon, k_{\parallel})$ without any impurity. The calculations are performed at zero temperature as no temperature dependence of the EC has been reported even at temperature $T_{\text{V}} = 120$ K, at which a charge and/or orbital ordered state appears.^{42–45}

C. Self-energy due to impurity

We introduce random impurities and in-gap states into the L and R interfaces of the junction, respectively. Randomness is expressed in terms of local self-energy $\Sigma_{\text{L(R)}\sigma}(z)$ after taking a suitable averaging procedure. Vertex corrections for the product of two Green's functions may be neglected in the lowest order of the disorder effects.⁴⁷

Magnetic impurities on the interface of L-FM (Fe), are treated in the Anderson model, in which the impurity level of up- and down-spin states is determined self-consistently via a relationship $V_{\text{imp}\sigma} = V_{\text{imp}} + U n_{\text{imp}}^{-\sigma}$, where V_{imp} , U , and n_{imp}^{σ} are the bare potential of the impurity, Coulomb repulsion on the impurity, and number of electrons with spin σ in the impurity, respectively. The number of electrons is determined by integrating the impurity Green's function $g_{\text{imp}\sigma}(z)$ as

$$n_{\text{imp}}^{\sigma} = -\frac{1}{\pi} \int^{\varepsilon_{\text{F}}} g_{\text{imp}\sigma}(z) d\varepsilon,$$

with

$$g_{\text{imp}\sigma}(z) = \frac{1}{z - V_{\text{imp}\sigma} - \gamma^2 g_{\text{L}\sigma}(z)},$$

where γ stands for the band mixing between the impurity and host matrix. The self-energy may be approximated as

$$\Sigma_{\text{L}\sigma}(z) \sim c_{\text{imp}} \gamma^2 g_{\text{imp}\sigma}(z),$$

with impurity concentration c_{imp} .

Because the in-gap state appears within the energy band gap, a simple treatment using such as the Anderson model gives a δ -function type state within the energy gap. To make the electronic states of the in-gap state more realistic, we adopt the average T -matrix approximation⁴⁸ for the in-gap state, the spin-dependent potential being given by $V_{\text{imp}\sigma}$. The self-energy is then given as

$$\Sigma_{\text{R}\sigma}(z) = \frac{c_{\text{imp}} V_{\text{imp}\sigma}}{1 - (1 - c_{\text{imp}}) V_{\text{imp}\sigma} g_{\text{R}\sigma}(z)}. \quad (5)$$

In the above expressions, the local Green's function $g_{\xi\sigma}(z)$ ($\xi = \text{L, R}$) of the surface is given as

$$\begin{aligned} g_{\xi\sigma}(z) &= \frac{1}{N} \sum_{k_{\parallel}} g_{\xi\sigma}(z, k_{\parallel}) \\ &= \int d\varepsilon \frac{D_0(\varepsilon)}{z - \varepsilon_{\xi\sigma} - \varepsilon - t^2 g_{\xi\sigma}(z, \varepsilon)}, \end{aligned} \quad (6)$$

by using a two-dimensional DOS,

$$D_0(\varepsilon) = \frac{2}{(4t)^2 \pi} \sqrt{\varepsilon^2 - (4t)^2}, \quad (7)$$

for simplicity. The bandwidth of the two-dimensional DOS is $8t$ and that of bulk lattice is $12t$.

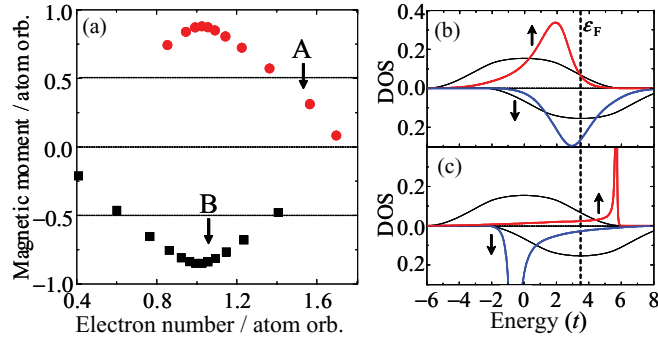


FIG. 6. (Color online) (a) Magnetic moments of impurities as calculated by the Anderson model, (b) local DOS of Co impurity indicated by an arrow A, and (c) local DOS of Cr or Mn impurity indicated by an arrow B. Thin curves denote the surface DOS of Fe.

D. Parameters

The relative position of the bands of L-FM and R-FM is determined in the following way. Because L-FM and R-FM correspond to ferromagnetic Fe and half-metallic Fe_3O_4 , the number of electrons and magnetic moment of L-FM are $7.2/5 = 1.44$ and $2.2/5 = 0.44$ per atom and orbital, respectively, and the magnetic moment of R-FM is the same as the electron number, i.e., $1/5$ per atom and orbital. Using these values, we determine $\epsilon_{L+} \equiv 0, \epsilon_{L-} = 3.5, \Delta = 3.5, \epsilon_F = 3.5$, and $\epsilon_{R-} = 5.0$, in units of t . An insulating state of R-FM may be obtained by taking a larger value of ϵ_{R-} than 9.5.

Values of γ and U in the Anderson model are taken to be 1.5 and 6 to reproduce reasonably the magnetic moments obtained in the first-principles calculations. The value of V_{imp} in the Anderson model is considered a variable to calculate a relationship between the magnetic moment and electron number of the impurity. The position of the in-gap state of R-FM is assumed to be $V_{\text{imp-}} = 0.0$ near the band bottom of the minority spin state of the R-FM.

IV. RESULTS OF MODEL CALCULATIONS

A. Impurity states

Calculated results of magnetic moments and local DOS of impurities are shown in Figs. 6(a)–6(c). In general, the impurity has two self-consistent solutions with positive and negative moments. The former (latter) is stable for high (low) electron number of the impurity. After multiplying by a factor five for the d orbitals, the magnetic moment shown with an arrow A is about $1.5 \mu_B$ per atom, corresponding to a Co impurity, and that shown an arrow B is about $-4.2 \mu_B$ per atom corresponding to a Cr or Mn impurity. Hereafter, we refer to the impurity indicated by arrows A (B) as A (B)-type impurity.

Local DOSs of A- and B-type impurities are shown in Figs. 6(b) and 6(c), respectively. Because the magnetic moment of A-type impurity is small, the exchange splitting is weak and the local DOS hybridizes with the host band resulting in a broad local DOS of both up and down spin states. On the other hand, local DOS of B-type impurity splits strongly due to the large negative moment and forms a sharp DOS as it locates near the edge of the host DOS. Existence of a broad s band in

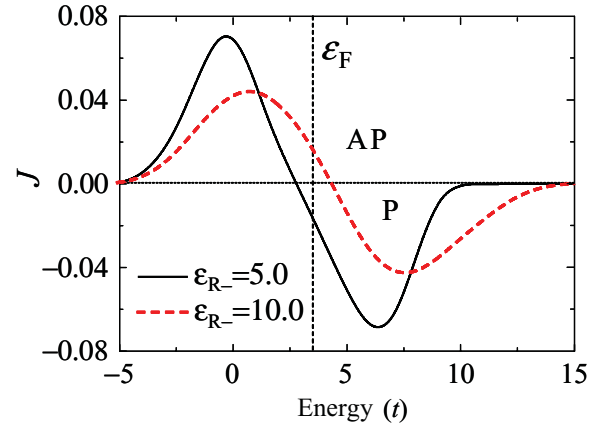


FIG. 7. (Color online) Calculated results of the exchange coupling J in units of t_{LR}^2/t for junction without impurities for $\epsilon_{R-} = 5.0$ and 10.0.

real Fe bands may cause the broadening of the local DOS. Thus we may conclude that the model calculations qualitatively reproduce the results obtained in the first-principles method.

B. Intrinsic exchange coupling

Figure 7 shows calculated results of J (in units of t_{LR}^2/t) as a function of energy (in units of t) for $\epsilon_{R-} = 5.0$ and 10.0. Positive (negative) values of J correspond to an AP (P) alignment of the L and R magnetizations. J is zero outside the whole band of the junction and changes sign near the center of the band. Because J is given by an energy integral of the imaginary parts of a product of two surface Green's functions of L-FM and R-FM, the EC is related to the energy dependence of both real and imaginary parts of the Green's function. Although DOS (imaginary part of the Green's function) is positive for all energy regions, the real part of the Green's function ($\text{Re}G$) may change sign with energy, as can be seen from the simplest form of the Green's function:

$$g(\epsilon + i\delta) = \frac{1}{\epsilon + i\delta - V_i} = \frac{\epsilon - V_i - i\delta}{(\epsilon - V_i)^2 + \delta^2}. \quad (8)$$

Therefore, a change in local DOS and $\text{Re}G$ affects both the sign and magnitude of J .

For junctions in which the difference between the electronic state of L and R layers is characterized by only the band position, the energy integration in Eq. (2) is performed easily resulting in

$$J = t_{\text{LR}}^2 \left(-\frac{n_{L+} - n_{R-}}{\epsilon_{L+} - \epsilon_{R-}} + \frac{n_{L-} - n_{R-}}{\epsilon_{L-} - \epsilon_{R-}} \right), \quad (9)$$

without explicit effects of $\text{Re}G$. When the Fermi energy is located near the bottom of the whole band, $n_{L+} \neq 0$, and $n_{L-} = n_{R-} = 0$, and $J > 0$ as $\epsilon_{L+} < \epsilon_{R-}$. When the Fermi energy is located near the top of the whole band, $n_{L+} = n_{L-} = 1$ and $n_{R-} < 1$, and $J < 0$, as $\epsilon_{L+} < \epsilon_{L-} < \epsilon_{R-}$. Thus we may understand the energy dependence of J shown in Fig. 7.

It is noted that $|J|$ may be small for the junctions we are dealing with because the Fermi energy is located near the center of the whole band of the junction. When the position of R-FM band is shifted to $\epsilon_{R-} = 10.0$, it becomes insulating,

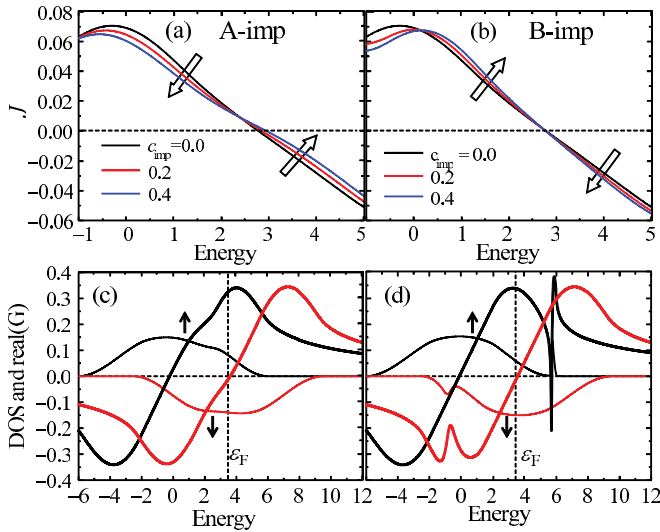


FIG. 8. (Color online) Calculated results of J in units of t_{LR}^2/t for impurity concentration $c_{imp} = 0.0, 0.2$, and 0.4 of (a) A-type impurity and (b) B-type impurity on L-FM interface. Tendency of the change in J is indicated by arrows. (c) and (d) are the corresponding local DOS (thin curves) and real part of the Green's function (thick curves) in up (\uparrow) and down (\downarrow) spin states with $c_{imp} = 0.2$.

and the value of J extends to higher energy as shown by the red broken curve. The result indicates that the P alignment at the Fermi energy $\varepsilon_F = 3.5$ for half-metallic R-FM becomes an AP alignment for insulating R-FM.

C. Extrinsic exchange coupling

Figures 8(a) and 8(b) show the change in J caused by introducing A- and B-type impurities in L-FM interface, respectively, as a function of energy. With increasing impurity concentration c_{imp} of A- and B-type impurities, the value of J changes systematically but in the opposite direction, as shown by arrows in Figs. 8(a) and 8(b). Furthermore, the degree of change in J seems to be larger for A-type impurity than for B-type one. The tendency may be explained in terms of the change of the electronic states (local DOS and ReG) at the interface caused by impurities as follows.

Figures 8(c) and 8(d) show the local DOS (thin curves) and real part of the Green's function ReG (thick curves) at the interface including A- and B-type impurity with $c_{imp} = 0.2$, respectively. We see in Fig. 8(c) that both the local DOS and ReG with A-type impurity are modified in an energy range between ~ 0 and ~ 5 from the unperturbed ones. This is because the impurity states appear around $\varepsilon \sim 2$ and 3 for majority and minority spin states, respectively. The change in local DOS and ReG by B-type impurity, on the other hand, occurs near $\varepsilon \sim 0$ for the minority spin states and $\varepsilon \sim 6$ for the majority spin states because of strong exchange splitting of the impurity states as shown in Fig. 6(c).

Because the weight of the local DOS of A-type impurity is large around $\varepsilon \sim 2-3$, the energy integral in Eq. (2) up to $\varepsilon \sim 2-3$ decreases, while it increases above $\varepsilon \sim 2-3$, as shown in Fig. 8(a). In addition, change in the electronic states in both the majority and minority spin states contribute to a large change in magnitude of J .

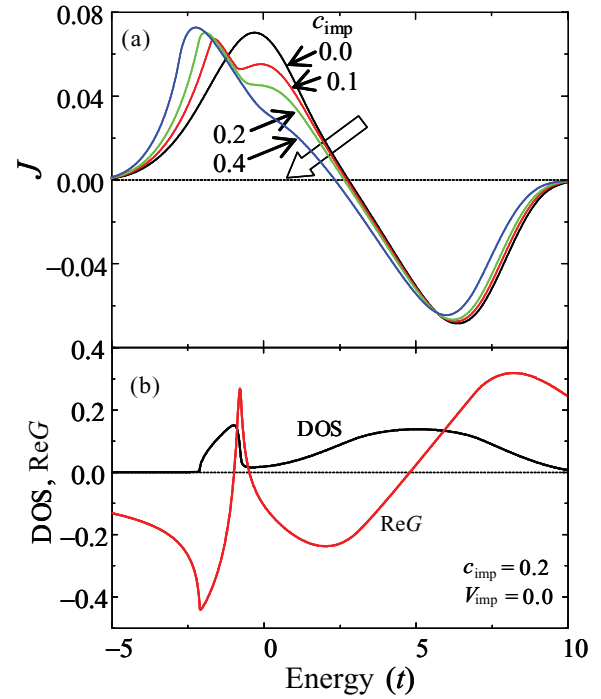


FIG. 9. (Color online) (a) Calculated results of J in units of t_{LR}^2/t as a function of energy for junctions with in-gap states at R-FM interface, and (b) local DOS and ReG at R-Fe interface.

Although the modification in the local DOS and ReG by B-type impurity is large at the bottom of the minority spin states of L-FM, it diminishes at energy near the Fermi level. The energy integration for J compensates the large modification in the electronic states, resulting in a small value of J near the Fermi level. Contribution to the change in the majority state becomes large when the energy integration is performed up to ~ 6 .

The difference between the tendency of increase/decrease in J caused by A- and B-type impurities is related to the difference between the energy regions where large modification occurs in the electronic states. Thus we may conclude that the difference of the tendency in the change in J due to impurities may be attributed to the change in the electronic states of impurities rather than to the sign and magnitude of the local moment of impurities, at least for a region of low impurity concentration. It may be noted that the appearance of energy at which J is independent of c_{imp} may be due to an approximate treatment of the impurity concentration for the self-energy. Inclusion of higher order of c_{imp} in the self-energy may remove this effect.

Effects of the in-gap state at R-FM interface on J are larger than those of magnetic impurities at L-FM interface, as shown in Fig. 9(a). The large change in J near $\varepsilon \sim 0$ is caused by a strong modification in both the local DOS and ReG as shown in Fig. 9(b). However, the change in J becomes small near the Fermi level because the effect of the change in the electronic state is weak near the Fermi energy. When the in-gap state appears near the Fermi level, the effect naturally becomes large. An interesting result is a tendency of the AP alignment changing to P alignments near $\varepsilon \sim 2.5$, which will be discussed further in the next section. Finally, it has been confirmed numerically that existence of both the magnetic

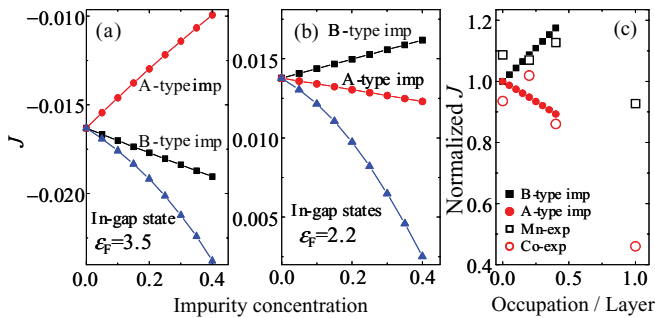


FIG. 10. (Color online) Calculated results of the exchange coupling J in units of t_{LR}^2/t for junctions with impurities on the left electrode with (a) fixed Fermi energy $\varepsilon_F = 3.5$ and (b) with a Fermi energy shifted to $\varepsilon_F = 2.2$. (c) Normalized exchange coupling shown in (b) with experimental results for Mn and Co impurities on Fe interface.¹⁴

impurities on Fe interface and the in-gap states in magnetite interface additively contribute to the EC of Fe/Fe₃O₄ in the present model.

V. DISCUSSIONS

We compare the calculated results of EC with the experimental ones for Fe/Fe₃O₄, Fe/ γ -Fe₂O₃, and Fe/Fe₃O₄ junctions with A-type (Co) or B-type (Mn) impurities at the interface. Fe/Fe₃O₄ junction shows AP alignment with $J \sim 1 \text{ erg/cm}^2 \sim 0.2 \text{ meV/atom}$, while Fe/ γ -Fe₂O₃ shows P alignment the value of J being unknown. The calculated value of J is of the order $0.01t_{LR}^2/t$ where $t \sim 0.5 \text{ eV}$. Therefore when $t_{LR} \sim 0.2t$, J is about 0.2 meV in agreement with the experimental value. The value of t_{LR} may not be unreasonable when we note that the interface of the Fe/Fe₃O₄ junction is rather electrically resistive. In reality, the small value of t_{LR} might be brought about by a structural disorder at the interface. Once the structural disorder is identified for example using STEM (scanning tunneling electron microscopy), more elaborate first-principles calculations can be performed to explain the observed values of the EC.

Figure 10(a) shows the dependence of J on the impurity concentrations of A- and B-type impurities and the in-gap states when the Fermi energy is located at $\varepsilon_F = 3.5$, as determined in the model. The results indicate that the undoped Fe/Fe₃O₄ junction is in P alignment, and the P alignment is weakened (strengthened) by A-type (B-type) impurity. This is contrary to the observed results¹⁴ in which the undoped

Fe/Fe₃O₄ junction shows AP alignment which is strengthened (weakened) by a small amount of Mn (Co) impurity. However, by shifting the Fermi energy to $\varepsilon_F = 2.2$, we obtain the results shown in Fig. 10(b) which reproduce the tendency in observed values. More explicitly, normalized values of J are compared with experimental ones in Fig. 10(c). On the other hand, the role of the in-gap states is nearly independent of the position of the Fermi energy: it makes the AP alignment weak, and possibly changes the AP alignment to P alignment, as observed in Fe/ γ -Fe₂O₃. We expect the role of the in-gap states to be large in Fe/ γ -Fe₂O₃ junctions because the samples are fabricated under oxygen-excess atmosphere. Considering that the crudeness of the model may produce an ambiguity in the position of the Fermi energy, the present model captures the fundamental nature of the effects of impurity on the EC, and may give a reasonable explanation for the change in EC observed for Fe/Fe₃O₄ with impurities at the interface.

Because the magnetic moment of A-site Fe is antiparallel to the total magnetic moment of Fe₃O₄, the in-gap states of A-site Fe appear in the down spin state when the magnetizations of Fe and Fe₃O₄ are in AP alignment. The situation is opposite to that considered in the model calculations in which the in-gap states appear in the down spin state when the magnetizations of Fe and Fe₃O₄ are in P alignment. Therefore the in-gap states in A-site Fe may weaken the tendency caused by the in-gap states in B-site Fe. However, the effect may not be sufficiently large to reverse the trend observed in the present calculations, because B-site Fe contact with the Fe layer in Fe/Fe₃O₄ junctions is more plausible than A-site Fe contact with the Fe layer.

Finally, let us discuss the effects of a MgO layer inserted between Fe and Fe₃O₄ or γ -Fe₂O₃ layer. Recent studies with the first-principles method for Fe/MgO/Fe junctions reported that an ideal MgO layer can weaken the P alignment exponentially with increasing MgO thickness, while an oxygen deficient MgO layer makes the coupling AP.^{23–25} Figures 11(a) and 11(b) reproduce the previous results of the EC in Fe/MgO/Fe junctions, with a new result of AP coupling due to Mg defects. Thus the excess oxygen at Fe₃O₄ interface and within MgO layer result in an opposite tendency on the EC, i.e., increase in the P (AP) coupling by the former (latter). In-gap states at Fe₃O₄/MgO interface, calculated recently with the first-principles method,⁴⁹ might also affect EC. We presume that the observed AP coupling in both Fe/MgO/Fe₃O₄ and Fe/MgO/ γ -Fe₂O₃ junctions might be realized by a complicated combination of these effects.

We have used simple models for the junction structure and magnetic impurities because of unidentified structural disorder at the interface of the oxide junctions. The results, however, have clarified the role of impurities on the EC from a microscopic viewpoint, at least qualitatively. Once the structural disorder is identified experimentally, one will be able to construct more realistic models for first-principles calculations. More quantitative study of EC using, e.g., the coherent potential approximation for clean junctions made of, for example, magnetic semiconductors¹⁷ will be a future issue.

VI. CONCLUSION

Using the results of the first-principles calculations for the magnetic and electronic states of impurities at Fe surface

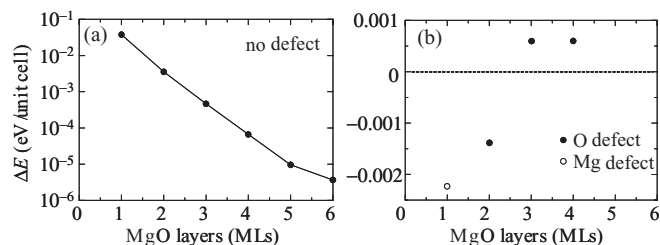


FIG. 11. Calculated results of the difference in the coupling energy ΔE between parallel and antiparallel alignment of the magnetization in Fe/MgO/Fe junctions (a) without and (c) with defects.

and for the electronic state of maghemite (γ -Fe₂O₃), we proposed a simple model of the exchange coupling in Fe/Fe₃O₄ junctions and performed model calculations to understand the effects of impurities on the exchange coupling. We have shown the following: the EC is weak when the Fermi energy is located near an energy region where the sign of J changes, Co and Cr (or Mn) impurities results in an opposite tendency for the change in J , and the in-gap states tend to make the coupling P aligned. The effect of the impurities may be explained in terms of the change in the

electronic states. Although the model is simple, we believe it captures the essence of the EC in Fe/Fe₃O₄ junctions. The present analysis suggests that magnetic coating of the interface could be useful for controlling the EC between two ferromagnets.

ACKNOWLEDGMENTS

This work was partly supported by Elements Science and Technology Projects of MEXT, Japan.

-
- ¹S. S. P. Parkin, N. More, and K. P. Roche, *Phys. Rev. Lett.* **64**, 2304 (1990).
- ²See, e.g., B. Heinrich, *Exchange Coupling in Magnetic Multilayers in Magnetic Heterostructures*, edited by H. Zabel and S. D. Bader, Springer Tracts in Modern Physics Vol. 227 (Springer, 2008).
- ³W. H. Meiklejohn and C. P. Bean, *Phys. Rev.* **102**, 1413 (1956).
- ⁴See e.g., F. Radu and H. Zabel, *Exchange Bias Effect of Ferro-/Antiferromagnetic Heterostructures in Magnetic Heterostructures*, edited by H. Zabel and S. D. Bader, Springer Tracts in Modern Physics Vol. 227 (Springer, 2008).
- ⁵J. C. Slonczewski, *Phys. Rev. B* **39**, 6995 (1989).
- ⁶D. M. Edwards, J. Mathon, R. B. Muniz, and M. S. Phan, *Phys. Rev. Lett.* **67**, 493 (1991).
- ⁷P. Bruno and C. Chappert, *Phys. Rev. Lett.* **67**, 1602 (1991).
- ⁸H. Yanagihara, Y. Toyoda, and E. Kita, *J. Appl. Phys.* **101**, 09D101 (2007).
- ⁹H. Yanagihara, Y. Toyoda, A. Ohnishi, and E. Kita, *Appl. Phys. Exp.* **1**, 111303 (2008).
- ¹⁰H. Yanagihara, Y. Toyoda, and E. Kita, *J. Phys. D: Appl. Phys.* **44**, 064011 (2011).
- ¹¹R. Skomski and J. M. D. Coey, *Phys. Rev. B* **48**, 15812 (1993).
- ¹²J. Zhang, Y. K. Takahashi, R. Gopalan, and K. Hono, *Appl. Phys. Lett.* **86**, 122509 (2005).
- ¹³S. S. P. Parkin, *Phys. Rev. Lett.* **67**, 3598 (1991).
- ¹⁴H. Yanagihara *et al.* (unpublished).
- ¹⁵T. Kida, S. Honda, H. Itoh, J. Inoue, H. Yanagihara, E. Kita, and K. Mibu, *Phys. Rev. B* **84**, 104407 (2011).
- ¹⁶Y. Toga, H. Moriya, H. Tsuchiura, and A. Sakuma, *J. Phys. Conf. Ser.* **266**, 012046 (2011).
- ¹⁷M. Luo, Z. Tang, J. Zheng, Z. Q. Zhu, and J. H. Chu, *J. Appl. Phys.* **108**, 053703 (2010).
- ¹⁸D. Ogawa, K. Koike, S. Mizukami, M. Oogane, Y. Ando, T. Miyazaki, and H. Kato, *J. Magn. Soc. Jpn.* **36**, 5 (2012).
- ¹⁹H. Kronmüller, R. Fischer, R. Hertel, and T. Leineweber, *J. Magn. Mater.* **175**, 177 (1997).
- ²⁰S.-J. Lee, S. Sato, H. Yanagihara, E. Kita, and C. Mitsumata, *J. Magn. Mater.* **323**, 28 (2011).
- ²¹W. Kakeno, S. Honda, J. Inoue, and H. Itoh, *J. Magn. Soc. Jpn.* **34**, 92 (2010).
- ²²W. Kakeno, S. Honda, H. Itoh, and J. Inoue, *Phys. Rev. B* **82**, 014413 (2010).
- ²³J. Faure-Vincent, C. Tiusan, C. Bellouard, E. Popova, M. Hehn, F. Montaigne, and A. Schuhl, *Phys. Rev. Lett.* **89**, 107206 (2002).
- ²⁴M. Ye. Zhuravlev, E. Y. Tsymbal, and A. V. Vedyayev, *Phys. Rev. Lett.* **94**, 026806 (2005).
- ²⁵T. Katayama, S. Yuasa, J. Velev, M. Ye Zhuravlev, S. S. Jaswal and E. Y. Tsymbal, *Appl. Phys. Lett.* **89**, 112503 (2006).
- ²⁶A. Yanase and K. Shiratou, *J. Phys. Soc. Jpn.* **53**, 312 (1984).
- ²⁷Z. Zhang and S. Satpathy, *Phys. Rev. B* **44**, 13319 (1991).
- ²⁸H. Yanagihara, M. Hasegawa, E. Kita, Y. Wakabayashi, H. Sawa, and K. Siratori, *J. Phys. Soc. Jpn.* **75**, 054708 (2006).
- ²⁹J. d'Albuquerque e Castro M. S. Ferreira, and R. B. Muniz, *Phys. Rev. B* **49**, 16062 (1994).
- ³⁰P. Bruno, *Phys. Rev. B* **49**, 13231 (1994).
- ³¹J. Mathon, M. Villeret, R. B. Muniz, J. d'Albuquerque e Castro, and D. M. Edwards, *Phys. Rev. Lett.* **74**, 3696 (1995).
- ³²D. M. Edwards, A. M. Robinson, and J. Mathon, *J. Magn. Mater.* **140-144**, 517 (1995).
- ³³J. d'Albuquerque e Castro, J. Mathon, M. Villeret, and A. Umerski, *Phys. Rev. B* **53**, R13306 (1996).
- ³⁴G. Kresse and D. Joubert, *Phys. Rev. B* **59**, 1758 (1999).
- ³⁵I. A. Campbell and A. A. Comès, *Proc. Phys. Soc.* **91**, 319 (1967).
- ³⁶T. Jo and H. Miwa, *J. Phys. Soc. Jpn.* **40**, 706 (1976).
- ³⁷R. Zeller, *Inst. of Phys. Conf. Ser.* **55**, 265 (1981).
- ³⁸See, e.g., P. Dederichs *et al.*, *J. Magn. Mater.* **100**, 241 (1991).
- ³⁹J. Kudrnovský, I. Turek, V. Drchal, P. Weinberger, S. K. Bose, and A. Pasturel, *Phys. Rev. B* **47**, 16525 (1993).
- ⁴⁰R. Grau-Crespo, A. Y. Al-Baitai, I. Saadoun, and N. H. De Leeuw, *J. Phys. Condens. Matter* **22**, 255401 (2010).
- ⁴¹R. Arras, L. Calmels, and B. Warot-Fonrose, *Appl. Phys. Lett.* **100**, 032403 (2012).
- ⁴²J. W. Verway and P. W. Haayman, *Physica* **8**, 979 (1941).
- ⁴³J. P. Wright, J. P. Attfield, and P. G. Radaelli, *Phys. Rev. Lett.* **87**, 266401 (2001).
- ⁴⁴I. Leonov, A. N. Yaresko, V. N. Antonov, M. A. Korotin, and V. I. Anisimov, *Phys. Rev. Lett.* **93**, 146404 (2004).
- ⁴⁵H.-T. Jeng, G. Y. Guo, and D. J. Huang, *Phys. Rev. Lett.* **93**, 156403 (2004).
- ⁴⁶H. Yanagihara *et al.* (unpublished).
- ⁴⁷P. Bruno, J. Kudrnovský, V. Drechal, and I. Turek, *Phys. Rev. Lett.* **76**, 4264 (1996).
- ⁴⁸R. J. Elliot, J. A. Krumhansl, and P. L. Leath, *Rev. Mod. Phys.* **46**, 465 (1974).
- ⁴⁹R. Arras, L. Calmels, and B. Warot-Fonrose, *J. Phys. Conf. Ser.* **200**, 072008 (2010).